

Counterion-Induced Abnormal Slowdown of F-Actin Diffusion across the Isotropic-to-Nematic Phase Transition

Jun He, Jorge Viamontes, and Jay X. Tang*

Department of Physics, Brown University, Rhode Island 02912, USA

(Received 30 March 2007; published 9 August 2007)

We report an abnormal slowdown of the longitudinal diffusion of *F*-actin across the isotropic-to-nematic phase transition region. To probe the underlying physics of this counterintuitive discovery, we compared the diffusion of *F*-actin, microtubules and fd virus in *F*-actin solutions across the transition region and found the *F*-actin diffusion markedly different from the other two filament types. Also, the viscous drag probed by *F*-actin was found to increase sharply with $[Mg^{2+}]$ in the nematic but not in the isotropic state. Based on the experimental results, we propose that the abnormal slowdown is caused by the weak electrostatic attraction between actin filaments in the nematic phase, in which neighboring filaments in parallel associate with each other transiently as they collide due to thermal fluctuations.

DOI: 10.1103/PhysRevLett.99.068103

PACS numbers: 87.15.Vv, 64.70.Md, 87.16.Ka

Actin is an abundant cytoskeletal protein in most eukaryotic cells and is responsible for their shape and motility. Monomeric actin (*G*-actin) polymerizes at physiological salt concentrations (e.g., 50 mM KCl and 2 mM $MgCl_2$) to form long actin filaments (*F*-actin). *F*-actin has a persistence length of 15–18 μm [1,2] and a diameter of 8 nm [3]. For protein concentration up to a few mg/ml, actin filaments are entangled to form an isotropic network, covering both semidilute and concentrated regimes. Above a threshold concentration, *F*-actin solution undergoes an isotropic (*I*) to nematic (*N*) liquid crystalline phase transition [4]. The order parameter of *F*-actin solution in the *N* phase has recently been measured to be about 0.75 [5,6], which implies imperfect alignment of actin filaments. In this Letter, we report a surprising slowdown of longitudinal diffusion of *F*-actin across the region of *I*-*N* phase transition, based on a microscopic study of filament motion.

To gain insight into the motion of *F*-actin in concentrated solutions, we tracked the motion of a small number of fluorescently labeled actin filaments in unlabeled background *F*-actin solutions [6]. The ratio of labeled to unlabeled filaments was below 1:1000. The average length of *F*-actin was regulated by adding gelsolin to *G*-actin before initiating polymerization. We calculated the average filament length as $\bar{l}(\mu\text{m}) = r_{AG}/370$ [7], where r_{AG} is the molar ratio of *G*-actin to gelsolin. Antiphotobleaching buffer was added to allow for longer observation times [8]. From a time-lapse fluorescence movie, the coordinate information of the center of mass of individual filaments can be extracted. The lateral displacement is largely suppressed by the surrounding network of actin filaments, while the longitudinal displacement is approximately an order of magnitude greater than the lateral displacement [Fig. 1(a)]. In other words, each actin filament moves as if it were confined in a virtual tube. The tube model and the concept of reptation, initially introduced by P.G. de Gennes for polymer dynamics [9], have proven to be highly successful in describing the motion of macromole-

ular filaments in concentrated solutions, including *F*-actin [10]. This concept also applies to *F*-actin in the *N* phase, due to the imperfect alignment of long actin filaments. In this Letter, we focus on the longitudinal motion of *F*-actin.

For example, the inset of Fig. 1(b) shows the longitudinal mean square displacement (MSD) as a function of time of two filaments with contour lengths of 1.9 and 6.9 μm in

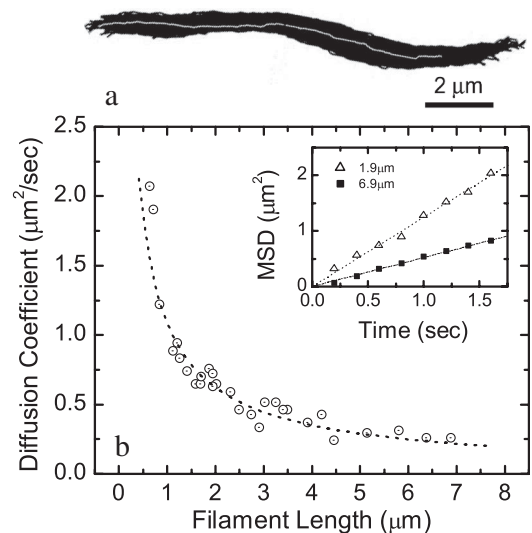


FIG. 1. (a) Overlay of the center threads of a single actin filament from a series of time-lapsed images. The white thread shows the initial position of the filament, with the later configurations added as black threads. This filament shows primarily a 1-D diffusion, as if being confined within a virtual tube. (b) A typical plot of the longitudinal diffusion coefficient of individual filaments vs. filament length (\odot). This solution has a concentration of 5.14 mg/ml and an average filament length $\bar{l} = 2.7 \mu\text{m}$. The dotted curve is the fit to Eq. (1) to obtain η_m . In this case, we find η to be 2.69 cP. The inset shows the longitudinal MSD of two representative filaments. The fit to $(\Delta X)^2 = 2Dt$ gives the diffusion coefficients for 1.9 μm (Δ) and 6.9 μm (\blacksquare) filaments, 0.72 and 0.30 $\mu\text{m}^2/\text{sec}$, respectively.

a solution with an actin concentration of 5.14 mg/ml and $\bar{l} = 2.7 \mu\text{m}$. The MSD follows the 1-D diffusion relation. By fitting the plot of MSD vs. time to $(\Delta X)^2 = 2D_{\parallel}t$, we obtain the longitudinal diffusion coefficients for these two filaments, which are 0.72 and 0.30 $\mu\text{m}^2/\text{sec}$, respectively. Performing the same analysis for filaments of different lengths, we obtain the diffusion coefficient as a function of filament length [Fig. 1(b)]. The drag coefficient ζ in the dilute limit of a straight rod is $\zeta = \rho\pi\eta L/\ln(L/d)$, where ρ is either 2 for longitudinal or 4 for lateral motions, respectively, η is the solvent viscosity, L is the filament contour length, and d is the filament diameter. The fit of the data to the Einstein relation

$$D_{\parallel} = k_B T / \zeta_{\parallel} = k_B T \ln(L/d) / 2\pi\eta L \quad (1)$$

with η as the only fitting parameter yields a microscopic viscosity, e.g., $\eta_m = 2.69 \text{ cP}$ for Fig. 1(b). It is worth noting that η_m only applies to longitudinal diffusion of F-actin and is very different from the bulk viscosity.

After measuring a range of actin concentrations, η_m is plotted against actin concentration across the I - N transition region for \bar{l} values of 2.7, 4, and 7 μm [Fig. 2(a)]. We also determined the transition region by measuring the optical birefringence for samples of corresponding \bar{l} . The specific retardance, which is proportional to the orientational order parameter, is shown in Fig. 2(b). A close comparison between Fig. 2(a) and 2(b) indicates that a marked increase in η_m occurs in the transition region for all three \bar{l} values. Samples with a shorter \bar{l} have a smaller increase. This means that the longitudinal diffusion slows down as the phase transition proceeds, which is abnormal and counterintuitive. In contrast to F-actin, for small molecule liquid crystals [11], rodlike polymer systems such as

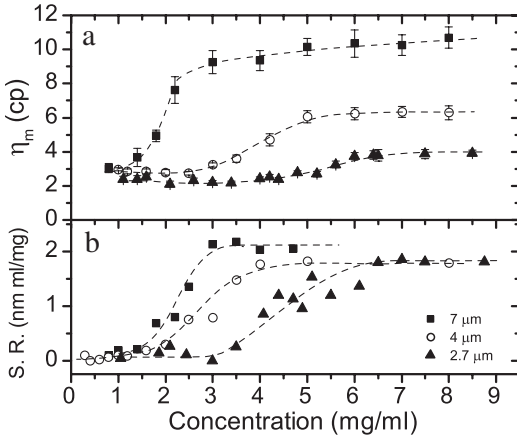


FIG. 2. (a) Microscopic viscosity η_m as a function of actin concentration across the I - N phase transition region is shown for three \bar{l} values of 2.7, 4, and 7 μm . All three series show a marked increase of η_m in the transition region. (b) The specific retardance (S.R.) is plotted against actin concentration across the same region. The increase of the order parameter (proportional to the specific retardance) is shown to be concurrent with the rise of η_m in the transition region.

PBLG [12], and fd virus solutions (\odot in Fig. 3), the longitudinal η_m decreases sharply in the I - N transition region. The reason for an increased diffusion in the N phase for the rodlike suspensions is usually ascribed to the tube dilation effect [13], which reduces the drag between the filament and the virtual tube wall defined by the surrounding filaments, thereby enhancing the diffusion.

To find the mechanism of this abnormal slowdown effect of F-actin, we compared the diffusion behaviors of F-actin, microtubules (MTs) and fd virus in F-actin solutions across the I - N transition region. Fd viruses are semiflexible filaments with a length of 0.88 μm , diameter of 6.6 nm, and persistence length of 2.2 μm [14,15]. MTs, another major component of the cytoskeletal network, have a diameter of 24 nm and a persistence length of several mms [2,16]. Fd viruses were fluorescently labeled with rodamine; MTs were labeled with oregon green taxol. The tracking of fd viruses or MTs in F-actin solution was carried out with the same procedure as that of F-actin. Figure 3 shows η_m probed by F-actin, MT, and fd virus as a function of actin concentration spanning the F-actin I - N transition region. These experiments were done using a background F-actin solution with $\bar{l} = 7 \mu\text{m}$. In Fig. 3, η_m of F-actin increases over 300% across the transition region. The increase of either fd virus or MT is about 20–30%, much smaller than that of F-actin. The different diffusion behaviors of these three probe macromolecules are likely caused by the difference among the interactions of actin-actin, MT-actin, and virus-actin.

We hypothesize that the electrostatic interaction between neighboring filaments is a key factor in the slowdown of the probe filaments, and the different charge properties cause the probe MT and fd to be affected much less. To support this idea, we measured η_m of F-

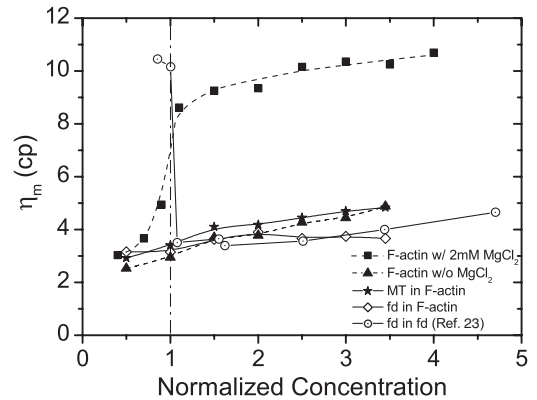


FIG. 3. The comparison of η_m of F-actin (\blacksquare), microtubules (\star) and fd virus (\diamond) in F-actin solutions with 50 mM KCl and 2 mM MgCl_2 across I - N phase transition. Also, the data of fd diffusion in fd solution, converted from Ref. [23], is presented as a comparison (\odot). In addition, η_m of F-actin in F-actin solutions with 50 mM KCl but no MgCl_2 is also shown (\blacktriangle). The concentrations are normalized with respect to the phase transition concentration. The normalized concentration of 1 stands for 2 mg/ml for F-actin and 15.5 mg/ml for fd, respectively.

actin vs. actin concentration in solutions without divalent counterions Mg^{2+} (Fig. 3). There is a substantial difference between F-actin solutions with (■) and without Mg^{2+} (▲). With 2 mM Mg^{2+} , the increase in η_m of F-actin is 3 times greater across the transition region. Without Mg^{2+} (there is always 0.2 mM Ca^{2+} in solution), the increase is reduced to under 50%, and the dependence of η_m on actin concentration is very similar to that probed by MTs (★). The slowdown effect diminishes without Mg^{2+} . This means that the abnormal slowdown is facilitated by the presence of divalent counterions.

The physical picture we propose is that the counterion mediated attraction between charged filaments (polyelectrolytes) results in the slowdown of filament diffusion in the N phase. When the filaments are parallel and very close, multivalent counterions, such as Mg^{2+} , condensed around these filaments can produce an effective attraction between them [17,18]. Such an attractive interaction can induce bundle formation when the counterion concentration reaches a threshold value [19]. Below that concentration, the attractive force is not strong enough to suppress the thermal fluctuations and bundle the filaments. It can, however, make neighboring filaments form a temporarily bound state when they approach the interacting range. Figure 4(a) illustrates the attraction between parallel actin filaments in the N phase. The divalent counterions act like bridges, causing two neighboring filaments to be attracted to each other and partially associate momentarily. In the I phase, the filaments exist in random orientations, so the counterion mediated attraction could only occur at their junction, which may be disrupted by the Brownian motion. Thus, this mechanism explains the concurrency of the slowdown of longitudinal diffusion with the orientational order.

This picture can qualitatively explain the different diffusion behaviors of F-actin, MT, and fd virus in F-actin solutions, based on the different charge densities of the three kinds of filaments. MTs and fd virus have more negative charges per unit length. They are more inclined to be repelled by actin filaments. It is known experimentally, for instance, that fd virus is less sensitive to $[\text{Mg}^{2+}]$: F-actin forms bundles at $[\text{Mg}^{2+}]$ about 25 mM [19], whereas fd virus forms bundles at about 60 mM Mg^{2+} [20]. In addition, since fd viruses are shorter and more flexible, it may be entropically more unfavorable for them to laterally associate with adjacent filaments [21]. This picture can also explain the result that shorter F-actin shows less slowdown [Fig. 2(a)]. Since shorter filaments are more inclined to rotate and less likely to accommodate parallel association, they experience less drag per unit length and hence a weaker slowdown effect.

Note in Fig. 3 that for MT (★) or fd virus (◇) diffusion in F-actin solution and F-actin diffusion without Mg^{2+} (▲) there is consistently a small slowdown instead of an increased diffusion as expected for rodlike systems across the I - N transition. We think that due to their long length and flexibility, F-actin in the N phase actually forms an

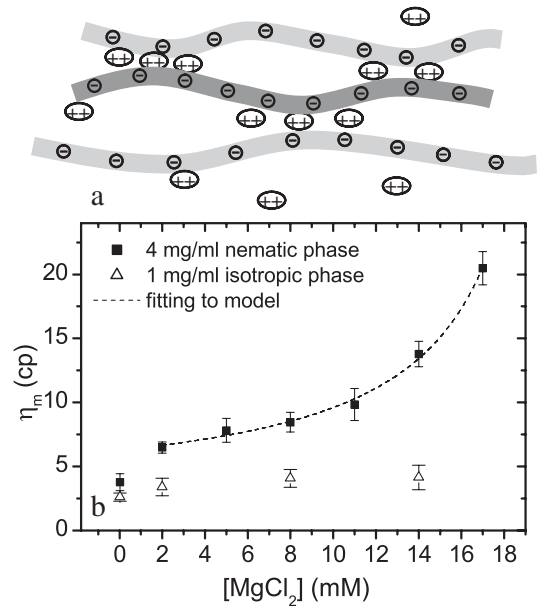


FIG. 4. (a) The illustration of weak attraction between actin filaments induced in the N phase by divalent counterions. The “-” symbols represent negative charges on F-actin, and the “++” symbols represent divalent counterions. The dark filament is confined in a virtual tube defined by its surrounding filaments. The divalent counterions temporarily associate parts of the filaments. (b) η_m of F-actin in the N phase (4 mg/ml) is plotted against $[\text{Mg}^{2+}]$ (■). The data in the I phase (1 mg/ml) is also shown (△). The fit to our model is given in the dashed line.

entangled network. One indicator is the imperfect alignment of F-actin in the N phase, with the order parameter significantly smaller than 1. Perhaps because of this imperfect alignment and entanglement in the N phase, the probe filaments continuously experience more drag with the increase of actin concentration even in the transition region. Thus, the entanglement diminishes the expected increase in the longitudinal diffusion of F-actin over the I - N transition region, whereas the steep increase in drag is due to the electrostatic interaction mediated by divalent counterions.

Based on this picture, we propose a simple model to explain how the slowdown phenomenon is affected by $[\text{Mg}^{2+}]$ in the N phase. The simplifying assumption of the model is that once a filament laterally associates with neighboring filaments, it stops moving for a time interval τ , which is assumed to follow an Arrhenius type behavior, i.e., $\tau = \tau_0 \exp[E(C_{\text{Mg}})/k_B T]$, where E is the activation energy for the filament to break the temporary binding. Assuming $E \propto C_{\text{Mg}}$, $\tau = \tau_0 \exp(AC_{\text{Mg}})$, where A is a pre-factor. The actual diffusion time is obtained by subtracting the time being stationary from the total time. The longitudinal diffusion equation becomes $(\Delta X)^2 = 2D_{\parallel 0}(t - nt \cdot \tau) = 2D_{\parallel 0}t$, where $D_{\parallel 0}$ is the diffusion coefficient without Mg^{2+} and n is the collision rate. Accordingly, we obtain an effective longitudinal diffusion coefficient $D_{\parallel} = D_{\parallel 0}(1 - n\tau)$. The effective microscopic viscosity

$\eta_m = (D_{||0}/D_{||})\eta_{m0} = \eta_{m0}/(1 - n\tau)$, i.e.,

$$\eta_m = \eta_{m0}/[1 - n\tau_0 \exp(AC_{Mg})]. \quad (2)$$

To test this model, we further measured η_m of F-actin with different $[Mg^{2+}]$ in both I and N phases. The dependence of η_m on $[Mg^{2+}]$ was measured for 4 mg/ml nematic F-actin solutions and 1 mg/ml isotropic solutions below the bundling concentration (about 20 mM) [Fig. 4(b)]. There is a 4 fold increase in η_m in the N phase when $[Mg^{2+}]$ rises from 0 mM to 17 mM. In contrast, η_m shows little change with the increase of $[Mg^{2+}]$ in the I phase. This means that $[Mg^{2+}]$ plays an important role in affecting F-actin diffusion in the N phase, but not in the I phase. Fitting the data in the N phase to Eq. (2) gives the values of the fitting parameters $\eta_{m0} = 3.78$ cP, $n\tau_0 = 0.41$, and $A = 0.04$ mM $^{-1}$ (dashed line in Fig. 4). With the fitted values of $n\tau_0$ and A , by setting $n\tau_0 \exp(AC_{Mg}) = 1$, we find $C_{Mg} = 22$ mM, which corresponds to the threshold concentration for bundle formation. This value agrees well with the experimental value of 20 mM under the ionic condition of this study, correctly predicting the onset of bundle formation.

We can further estimate the collision rate n based on the reptation dynamics and accordingly yield an estimate of τ_0 . First, we assume that the filament takes a sinusoidal form with an amplitude of the tube radius R , about 0.02 μ m for 4 mg/ml solution [22]. Integrating the bending energy over the filament contour and assigning a bending energy of $k_B T$ per wavelength λ of filament undulation, we find $\lambda \approx 1.5$ μ m. Presumably, the filament can be divided into segments with length λ , which laterally diffuse independently. The time for each segment to diffuse over a tube diameter is $t_D = 4R^2/D_{\perp}$, where D_{\perp} is the lateral diffusion coefficient, and $D_{\perp} = k_B T \ln(\lambda/d)/4\pi\eta\lambda$, with η being the viscosity of water (1 cP). Then, the collision rate $n = (1/t_D)(\bar{l}/\lambda)$, which is about 3500 s $^{-1}$ for 4 mg/ml F-actin with $\bar{l} = 7$ μ m. This leads to τ_0 being on the order of 0.1 ms. Based upon this estimation, we can also qualitatively explain the average length effect, i.e., F-actin with shorter \bar{l} has a smaller increase in η_m across the transition. A smaller \bar{l} corresponds to a smaller n , resulting in a smaller η_m from Eq. (2).

In summary, we discovered an abnormal increase in η_m of F-actin across the I - N phase transition. Furthermore, an increased $[Mg^{2+}]$ results in a larger slowdown. Entanglement in F-actin over the I - N transition region abolishes the expected increase in the longitudinal diffusion. The abnormal slowdown of F-actin is proposed to be primarily caused by the divalent counterion mediated attraction in the N phase. A simple model based on this picture quantitatively explains the effect of $[Mg^{2+}]$ on

the slowdown phenomenon and qualitatively accounts for the different behaviors among different probe filaments.

We thank Alex Levine, M. Muthukumar, and Yongxing Guo for the insightful discussions. This work is supported by the National Science Foundation (NSF No. DMR0405156) and the Petroleum Research Fund (PRF No. 42835-AC7), administered by the American Chemical Society.

*Jay_Tang@Brown.edu

- [1] H. Isambert, P. Vernier, A. C. Maggs, A. Fattoum, R. Kassab, D. Pantaloni, and M. F. Carlier, *J. Biol. Chem.* **270**, 11437 (1995).
- [2] F. Gittes, B. Mickey, J. Nettleton, and J. Howard, *J. Cell Biol.* **120**, 923 (1993).
- [3] K. C. Holmes, D. Popp, W. Gebhard, and W. Kabsch, *Nature (London)* **347**, 44 (1990).
- [4] J. Viamontes, P. W. Oakes, and J. X. Tang, *Phys. Rev. Lett.* **97**, 118103 (2006).
- [5] E. Helfer, P. Panine, M. Carlier, and P. Davidson, *Biophys. J.* **89**, 543 (2005).
- [6] J. Viamontes, S. Narayanan, A. R. Sandy, and J. X. Tang, *Phys. Rev. E* **73**, 061901 (2006).
- [7] P. A. Janmey, J. Peetermans, K. S. Zaner, T. P. Stossel, and T. Tanaka, *J. Biol. Chem.* **261**, 8357 (1986).
- [8] J. Käs, H. Strey, J. X. Tang, D. Finger, R. Ezzell, E. Sackmann, and P. A. Janmey, *Biophys. J.* **70**, 609 (1996).
- [9] P. G. de Gennes, *J. Chem. Phys.* **55**, 572 (1971).
- [10] J. Käs, H. Strey, and E. Sackmann, *Nature (London)* **368**, 226 (1994); F. C. Mackintosh, J. Kas, and P. A. Janmey, *Phys. Rev. Lett.* **75**, 4425 (1995); D. C. Morse, *Macromolecules* **31**, 7030 (1998); B. Hinner, M. Tempel, E. Sackmann, K. Kroy, and E. Frey, *Phys. Rev. Lett.* **81**, 2614 (1998).
- [11] S. V. Dvinskikh and I. Furó, *J. Chem. Phys.* **115**, 1946 (2001).
- [12] Z. Bu, P. S. Russo, D. L. Tipton, and I. I. Negulescu, *Macromolecules* **27**, 6871 (1994).
- [13] M. Doi and S. F. Edwards, *The Theory of Polymer Dynamics* (Oxford University Press, Oxford, 1986).
- [14] J. X. Tang and S. Fraden, *Liq. Cryst.* **19**, 459 (1995).
- [15] L. Makowski, *Virus Structure* (Wiley-Interscience, New York, 1984).
- [16] A. Desai and T. J. Mitchison, *Annu. Rev. Cell Dev. Biol.* **13**, 83 (1997).
- [17] F. Oosawa, *Polyelectrolytes* (Marcel Dekker, Inc., New York, 1971).
- [18] G. S. Manning, *J. Chem. Phys.* **51**, 924 (1969).
- [19] J. X. Tang and P. A. Janmey, *J. Biol. Chem.* **271**, 8556 (1996).
- [20] J. X. Tang, P. A. Janmey, A. Lyubartsev, and L. Nordenskiöld, *Biophys. J.* **83**, 566 (2002).
- [21] M. J. Stevens, *Phys. Rev. Lett.* **82**, 101 (1999).
- [22] D. C. Morse, *Phys. Rev. E* **63**, 031502 (2001).
- [23] M. P. Lettinga, E. Barry, and Z. Dogic, *Europhys. Lett.* **71**, 692 (2005).